
A BIOLOGICAL GROWTH METRIC FOR 3D SHAPE REGISTRATION

M.H-M. Syn and R.W. Prager

CUED/F-INFENG/TR 225

July 1995

Cambridge University Engineering Department
Trumpington Street
Cambridge CB2 1PZ
England

E-mail: mhs@eng.cam.ac.uk, rwp@eng.cam.ac.uk

Abstract

We review the Turing (1952) and Oster-Murray (1988) models of biological *morphogenesis*. From the latter we apply primary mechanisms of extracellular-matrix (ECM) deformation, cell mitosis, cell diffusion and ECM-cell interaction to a model of biological *growth*, and derive the principal modes of mass flux from the linear eigenmodes of each mechanism. The assumption of uniform mass distribution means that the eigenmodes are the same for elastic, diffusive and convective modes.

We derive a metric of biological growth using the Gompertz function and show that it can also be arrived at from a thermodynamic model of growth inhibition. This metric is to be used in 3D shape registration, and can be computed for partial local registrations using a linear sum of eigenmode projections.

Contents

1	Introduction	3
1.1	Prospectus	3
2	Biological morphogenesis	5
2.1	The Turing mechanism	5
2.1.1	Morphogenetic gradients	5
2.2	The Oster-Murray mechanism	8
2.2.1	Mechanochemical factors	8
2.3	Discussion	9
2.3.1	Branching and circular growth patterns	9
3	Modelling biological growth	11
3.1	Components of the growth process	11
3.1.1	Extracellular Matrix	11
3.1.2	Mesenchymal cells	12
3.1.3	Epithelial cells	12
3.1.4	Notation	13
3.2	ECM growth	13
3.2.1	Hydrostatic pressure	13
3.2.2	Mapping the wave equation to finite elements	15
3.3	Cell growth	16
3.3.1	Classical diffusion	16
3.3.2	Reaction-diffusion	17
3.3.3	Conservation of cell mass	17
3.3.4	Local redistribution of cells after mitosis	18
3.3.5	Principal modes of growth	18
3.4	Cell-ECM interaction	19
3.4.1	Principal modes of convection	20
3.5	Discussion	20

3.5.1	Physical parameters	20
4	Growth energy	22
4.1	The Gompertz growth function	22
4.2	Medawar's growth energy	23
4.3	Growth energy as a function of mass	23
4.4	Interpretation of growth energy metric	23
4.5	Computation of growth energy	24
4.6	Eigenmode energy	25
4.6.1	Statistical modes	26
4.7	Biological justification	28
4.7.1	Tumour growth models	28
4.7.2	Thermodynamic model	28
5	Discussion	30
5.1	Acknowledgements	30
	Bibliography	30

Chapter 1

Introduction

Mathematical biology aims to model the mechanisms involved in biological processes. In this report we examine the application of such models in developmental biology, since an understanding of the processes involved in the formation and growth of biological structures can aid in the interpretation of medical images. This is especially true in 3D ultrasound, which requires many constraints for the recovery of useful information from very noisy images (Syn & Prager 1994).

The study of embryology and morphogenesis in particular, examines possible explanations of how a single fertilized egg cell can divide and differentiate into many complex components. The mechanisms driving this morphogenesis are genetically controlled, but the genes themselves cannot create spatial patterns. One of the major problems in biology is how the genetic code is physically translated into the necessary pattern and form. Murray (1989) provides a detailed description of mechanisms of spatial pattern formation in biology. Levin & Segel (1985) provide a wide-ranging review of research in pattern formation.

Plausible models have been built of relatively simple systems in animal coat patterns, plant growth and tumour growth, and also in quite complex ecological systems.

1.1 Prospectus

Chapter 2

We review current research into proposed mechanisms of spatial pattern formation

Chapter 3

We consider the physical processes driving biological growth and shape change.

Chapter 4

We show that the Gompertz function is an appropriate model for organ growth, and derive a growth energy metric from it.

Chapter 2

Biological morphogenesis

2.1 The Turing mechanism

Turing (1952) studied pairs of reaction-diffusion equations, which are generally formulated as follows

$$\frac{\partial c_i}{\partial t} = h_i(c_1, \dots, c_n) + D_i \nabla^2 c_i \quad i = 1, \dots, n \quad (2.1)$$

where c_i is concentration and D_i is a constant diffusivity. He chose polynomial reaction functions h_1 and h_2 and found that under certain conditions, uniform solutions were unstable to small perturbations, and stable non-uniform spatial patterns could result. This is sometimes known in the literature as *symmetry-breaking*.

Turing's mechanism therefore demonstrates that since reaction-diffusion instabilities can lead to patterned distribution of chemicals, such distributions of chemical *morphogens* might underlie the creation of biological pattern.

Figure 2.1 shows pattern emergence in Young's (1984) activator-inhibitor (reaction-diffusion) system, with areas of high concentration (black) clustering as the system evolves. Figure 2.2 shows different final patterns achieved with different system parameters.

2.1.1 Morphogenetic gradients

Meinhardt & Klingler (1987) in their earlier work advanced similar ideas to Turing, with the emphasis on the combination of short-range *activation* and long-range *inhibition*. They pointed out that gradients of morphogens did not require pre-arranged sources and sinks. Their specific work on the control of head and foot regeneration in *hydra* has been confirmed by the recent chemical identification of morphogens in *hydra* (Gierer 1974).

Figure 2.3 shows a sample pattern generated by Meinhardt & Klingler's (1987) activator-inhibitor model. Figure 2.4 compares a digitised image with a model generated using another

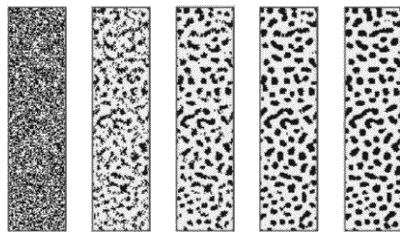


Figure 2.1: Pattern emergence in a reaction-diffusion system (Prusinkiewicz 1994)

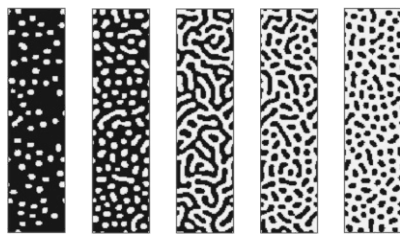


Figure 2.2: Patterns produced with different parameters (Prusinkiewicz 1994)

set of parameters.

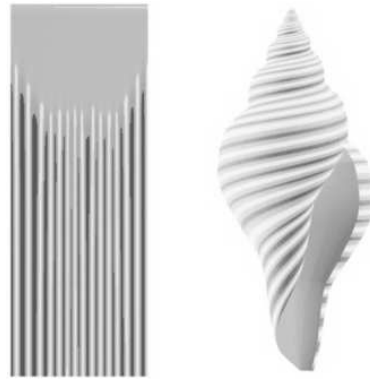


Figure 2.3: Sample pattern generated by the activator-inhibitor model (Prusinkiewicz 1994)



Figure 2.4: A photograph and model of *Amoria elhoti* (Prusinkiewicz 1994)

Wolpert (1978) proposed that cells differentiate according to positional information acquired by cells reacting to threshold levels of morphogen concentration. He demonstrates this mechanism in a number of experiments on embryo chicken wings.

More recently Hunding & Engelhardt (1995) used Turing's mechanism to model stripe pre-patterning and head formation in insect embryogenesis. Again this mechanism depends on morphogenetic gradients as the main source of positional information. They argue that being able to extract reliable positional information from a morphogenetic gradient, also makes the control system prone to yield pattern formation by symmetry-breaking processes

such as Turing's mechanism.

2.2 The Oster-Murray mechanism

Reaction-diffusion models show that a chemical pre-pattern can be established, which then activates the differentiation and growth of biological structures. Thus morphogenesis is a slave process which is determined once the chemical pattern has been established.

Shape changes in growing structures involve mechanical forces, which Murray, Maini & Tranquillo (1988) have shown to be intimately connected with the pattern formation process. The Oster-Murray mechanochemical approach differs from the chemical pre-pattern approach, in that pattern formation and morphogenesis proceed simultaneously.

One important benefit of simultaneous development is that such mechanisms can be self-correcting, whereas the Turing mechanism is effectively an open-loop system (Murray et al. 1988). In addition Goodwin, Kauffman & Murray (1993) have shown that the close coupling of different mechanisms reduces the number of degrees-of-freedom the coupled system has in converging upon a stable state. This implies a morphogenetic process which is robust to noise in genetic control parameters.

2.2.1 Mechanochemical factors

Murray et al.'s (1988) approach takes account of the coordinated patterning of mesenchymal and epithelial cells, which are two types of early embryonic cells (Moore 1982). Where standard Turing-type models consider the interaction of hypothetical morphogens, the Oster-Murray model is centred on the cell as the fundamental unit of biological growth. The model includes the effects of

- cell convection;
- short and long range diffusion of cells;
- cell proliferation rate;
- contact inhibition and guidance by neighbouring cells;
- haptotaxis (movement up an adhesive gradient);
- galvanotaxis (movement influenced by electric potentials);
- chemotaxis (movement influenced by chemical concentration gradients).

In other words, the cell flux term \mathbf{J} in the general cell-conservation equation

$$\frac{\partial c}{\partial t} = -\nabla \cdot \mathbf{J} + h_{mit} \quad (2.2)$$

is no longer merely localised diffusion (cf. Equation 2.1), but includes the mechano-chemical factors mentioned above. Note that c now refers to cell rather than morphogen concentration, and that the cell source term $h_{mitotic}$ can be a simple cell proliferation model (eg. logistic or Gompertz growth) rather than an activator-inhibitor expression.

Murray et al. (1988) and Murray (1989, Ch. 17.3) go on to perform linear analysis on a simplified model, and find that there are a large class of spatially inhomogeneous solutions, which are capable of producing spatial patterning similar to reaction-diffusion systems. A numerical simulation by Savic (1995) of pattern formation in animal coatings using a polarisation-elasticity model, gives very similar results to Meinhardt (1982).

2.3 Discussion

The Oster-Murray model is concerned solely with the aggregation and self-organisation of cells to form patterns as a basis for morphogenesis. Boundary conditions are essentially fixed so that the behaviour of temporally unstable waves can give rise to stable but spatially inhomogeneous solutions. The mechanisms are very general, although most of the physical parameters can in principle be experimentally determined, so until recently the Oster-Murray model has been applied in more qualitatively than computationally. Murray (1989) describes the pattern formation processes that accompany the formation of (mesenchymal) skin organ primordia for feathers, scales and teeth.

The significance of our model in Chapter 3 is that the (mesenchymal) cell is recognised as the fundamental unit of biological growth and shape change. This is implicit in the Oster-Murray model, although it is specifically applied to pattern formation.

We are interested to applying our model to the comparison of biological shapes using a growth energy metric, and show in Chapter 4 that growth energy is dependant only upon mass increase. This is exactly the premise of our model - mass change due to cell mitosis creates local changes in cell concentration, which drive the elastic, diffusive and convective mass redistribution mechanisms, resulting in boundary shape changes in the steady state. This model is general enough to apply across different organs which are generally of mesenchymal origin, and yet is specific enough to consider the cell as the origin of biological growth.

2.3.1 Branching and circular growth patterns

Trinkhaus (1984, Ch. 14) describes how morphogenetic movements in organogenesis are different for “circular” and “branching” structures. Both types of growth patterns occur in organ growth, and at the lowest level they must derive from the same growth mechanisms. It is unclear whether they share the growth and shape control mechanisms however.

In the case of *diffusion-limited growth* (Meakin 1986), which is limited by availability of nutrition or alternatively by presence of growth inhibitory factors, Matsushita & Fujikawa (1990) have shown in bacterial colonies that both circular and branching growth patterns can occur.

There are evolutionary, genetic, biological and random influences in growth and shape control mechanisms, which we have not included in our simple thermodynamic model of inhibitory control (see Section 4.7.2). In some biological structures such as the hand for instance, growth occurs by death of cells between fingers as much as cell growth and differentiation within fingers.

Chapter 3

Modelling biological growth

3.1 Components of the growth process

We aim to model generally the incremental growth of structures commonly scanned using 3D ultrasound. Organs such as the spleen, liver, kidney and gallbladder are of mesenchymal origin, and in this chapter we consider the major mechanisms of growth and cell transport in the Oster-Murray pattern formation model.

3.1.1 Extracellular Matrix

Mesenchymal cells secrete extracellular matrix (ECM) which forms part of the tissue within which cells move. The ECM is mainly made up of elastin and collagen which are two organic elastic materials, and is approximately linear elastic¹ for small strains. See Figure 3.1.

The ECM is not necessarily isotropic in its elastic properties, and Murray (1989, Ch. 17.2) presents a mechanism for inclusion of this effect, although he does not include it in the final model.

The time scale of incremental organ development is very long (hours) and the spatial scale is very small (millimetres), so that we can ignore inertial effects when considering cell-ECM interaction (Murray 1989, Ch. 17.2). We can also ignore effects of viscosity in the ECM, since the viscous component of the stress-strain relation² is

$$\sigma_{visc} \propto \frac{\partial \epsilon}{\partial t} \quad (3.1)$$

The properties of the ECM as a linear elastic substrate is modelled below in Section 3.2

¹Apropos Hooke's Law: Robert Hooke was also the one who first recognised and named the cell as a unit of living tissue.

²An earlier report (Syn & Prager 1995*b*) describes the modelling of elastic structures

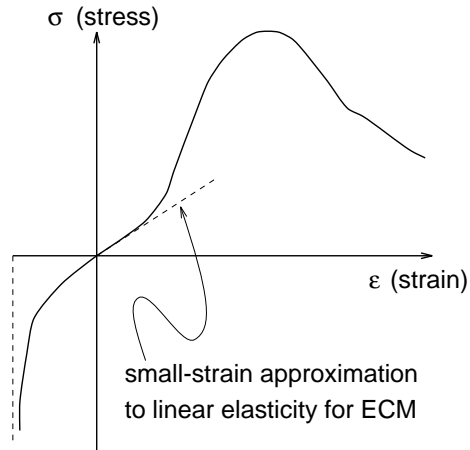


Figure 3.1: Schematic plot of ECM stress-strain behaviour (Murray 1989)

3.1.2 Mesenchymal cells

Mesenchymal cells move by exerting traction forces on the elastic fibrous ECM and the surface of other cells. As some cells move through the ECM, the anisotropically deforming ECM can convey other cells which are attached to it. This convection effect is modelled in Section 3.4

Cells proliferate by process of mitosis, the rate of which is usually modelled using a logistic function. Chapter 4 provides a review of literature which suggest the Gompertz function as a better model in certain circumstances. The growth in tissue mass due to mitosis results in local changes in cell concentration, which are equalised by local diffusion. This is discussed in Section 3.3.

3.1.3 Epithelial cells

Epithelial cells do not move about, but respond to forces exerted by mesenchymal cells by spreading or thickening. We can think of them as effecting shape control over the growing mesenchymal cell population.

Thus our simple model of organ growth has mesenchymal cells proliferating and causing the boundary layers of epithelial cells to shift in accomodation. With this shape growth comes a reorganisation of mass within the organ, using the mechanisms described above. We will show below how the mass flux during incremental organ growth can be described by a linear sum of eigenmodes.

As mentioned previously the time scale of the growth processes we are interested in is very long and the spatial scale very small, so that we can ignore transient responses and

consider only the steady-state spatial modes of mass flux.

3.1.4 Notation

We use \mathbf{x} as the spatial variable and t as the temporal one. The scalar u represents spatial displacement of the ECM, and c represents (displacement of) cell concentration.

We may for ease of notation also use \dot{y} to denote the temporal derivative of y , and y' to denote the spatial derivative.

We use the following 3D vector operator for gradient and divergence operations

$$\nabla = \left[\frac{\partial}{\partial x} \quad \frac{\partial}{\partial y} \quad \frac{\partial}{\partial z} \right]^T \quad (3.2)$$

3.2 ECM growth

The wave equation governs the behaviour of elastic structures³, and on the assumption of uniform mass and stiffness properties we have

$$\frac{\partial \mathbf{u}}{\partial t} = -D_{el} \nabla (\nabla \cdot \mathbf{u}) \quad (3.3)$$

which has a separation of variables solution

$$\mathbf{u}(\mathbf{x}, t) = \mathbf{f}_1(\mathbf{x}) g_1(t) \quad (3.4)$$

We have shown in an earlier report (Syn & Prager 1995*b*) that in the absence of damping $g_1(t)$ is a sinusoidal modulation, and $\mathbf{f}_1(\mathbf{x})$ can be computed for finite-element models to give the elastic FEM eigenmodes.

In reality the ECM does have damping which can be included in the FEM model using Rayleigh damping, which assumes the damping matrix to be a linear combination of the mass and stiffness matrices. However as mentioned previously the large time scale and small spatial scale of the growth processes we are looking at, means that damping can be ignored since it is a function of $\frac{\partial \mathbf{u}}{\partial t}$.

3.2.1 Hydrostatic pressure

Timoshenko & Goodier (1970, Ch. 1.7) defines the hydrostatic pressure p of an element to be the negative mean of its principal stresses

³Murray (1989, Ch 15.1) describes forced vibrations on thin plates with appropriate boundaries, which give similar results to the initial stages of reaction-diffusion pattern formation since there is only a small deviation from uniformity and hence a similar eigenproblem

$$p = -\frac{\tau_{xx} + \tau_{yy} + \tau_{zz}}{3} \quad (3.5)$$

The stress-strain relation in 3D for planar components is (Syn & Prager 1995*b*)

$$\boldsymbol{\tau} = \mathbf{E}\boldsymbol{\epsilon} \quad (3.6)$$

$$\begin{bmatrix} \tau_{xx} \\ \tau_{yy} \\ \tau_{zz} \end{bmatrix} = \frac{E(1-\nu)}{(1+\nu)(1-2\nu)} \begin{bmatrix} 1 & \frac{\nu}{1-\nu} & \frac{\nu}{1-\nu} \\ \frac{\nu}{1-\nu} & 1 & \frac{\nu}{1-\nu} \\ \frac{\nu}{1-\nu} & \frac{\nu}{1-\nu} & 1 \end{bmatrix} \begin{bmatrix} \epsilon_{xx} \\ \epsilon_{yy} \\ \epsilon_{zz} \end{bmatrix} \quad (3.7)$$

where E is the Young's Modulus and ν is the Poisson ratio. This means that hydrostatic pressure is directly dependant upon the local principal strain components⁴

$$p = -\frac{E}{(1-2\nu)} \frac{(\epsilon_{xx} + \epsilon_{yy} + \epsilon_{zz})}{3} \quad (3.8)$$

For an infinitesimal element, the strain vector $\boldsymbol{\epsilon} = \nabla \cdot \mathbf{u}$. Let us examine the vector components of $\mathbf{u} = \begin{bmatrix} u_x & u_y & u_z \end{bmatrix}^T$ in Equation 3.3

$$\begin{aligned} \frac{\partial}{\partial t} \begin{bmatrix} u_x \\ u_y \\ u_z \end{bmatrix} &= -D_{el} \nabla \left(\nabla \cdot \begin{bmatrix} u_x \\ u_y \\ u_z \end{bmatrix} \right) \\ &= -D_{el} \begin{bmatrix} \frac{\partial}{\partial x} \\ \frac{\partial}{\partial y} \\ \frac{\partial}{\partial z} \end{bmatrix} \left(\frac{\partial u_x}{\partial x} + \frac{\partial u_y}{\partial y} + \frac{\partial u_z}{\partial z} \right) \end{aligned} \quad (3.9)$$

Since u_x exists only in the x -direction

$$\frac{\partial^2}{\partial y \partial x} (u_x) = \frac{\partial^2}{\partial z \partial x} (u_x) = 0 \quad (3.10)$$

and similarly for u_y and u_z . Therefore Equation 3.9 becomes

$$\frac{\partial}{\partial t} \begin{bmatrix} u_x \\ u_y \\ u_z \end{bmatrix} = -D_{el} \begin{bmatrix} \frac{\partial^2}{\partial x^2} \\ \frac{\partial^2}{\partial y^2} \\ \frac{\partial^2}{\partial z^2} \end{bmatrix} \cdot \begin{bmatrix} u_x \\ u_y \\ u_z \end{bmatrix} \quad (3.11)$$

⁴The sum of principal strains is also known as the dilatation $\theta = \epsilon_{xx} + \epsilon_{yy} + \epsilon_{zz}$. This leads to a more intuitive explanation of pressure as the result of local compression or negative dilatation

and taking the mean of the spatial derivatives of the three vector components lets us write the scalar wave equation for hydrostatic pressure p

$$\frac{\partial p}{\partial t} = -D_{el}\nabla^2 p \quad (3.12)$$

This shows that there is a spatial pressure (or stress or mass concentration) distribution associated with each displacement eigenmode of the vector wave equation in Equation 3.3. These spatial fields are also eigenmodes

$$p(\mathbf{x}) = f_1(\mathbf{x})g_1(t) \quad (3.13)$$

3.2.2 Mapping the wave equation to finite elements

The *discrete* FEM governing equation for an undamped and unforced structure

$$\mathbf{M}\ddot{\mathbf{u}} = -\mathbf{K}\mathbf{u} \quad (3.14)$$

differs from the *continuous* wave equation

$$\frac{\partial^2 \mathbf{u}}{\partial t^2} = -D_{el}\nabla(\nabla \cdot \mathbf{u}) \quad (3.15)$$

in that Equation 3.14 has the right-hand term \mathbf{u} , where Equation 3.15 has $\nabla(\nabla \cdot \mathbf{u})$.

Let us examine the limiting behaviour of the discrete one-dimensional finite-element system in Figure 3.2 as the elements decrease in size.

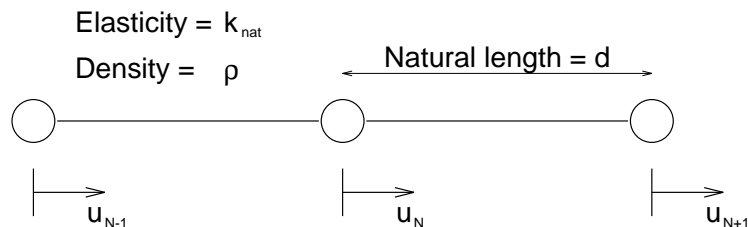


Figure 3.2: Discrete one-dimensional finite element system

Nodes are connected elastically to each other at natural length d , and elements have mass density ρ ⁵.

⁵It is simplest to have all elements at the same mass and natural length, so that in the limit the system tends straightforwardly to a continuum.

Consider the displacements u_{n-1} , u_n and u_{n+1} of three adjacent elements. The mass belonging to each node is ρd , with half the elemental contribution on each side. Then for natural elasticity k_{nat} the equilibrium equation is

$$\begin{aligned} \frac{k_{nat}(u_{n-1} + u_{n+1} - 2u_n)}{d} &= \rho d \ddot{u}_n \\ \frac{k_{nat}(u_{n-1} + u_{n+1} - 2u_n)}{d^2} &= \rho \ddot{u}_n \end{aligned} \quad (3.16)$$

In the limit as $d \mapsto 0$, we get

$$k_{nat} u'' = \rho \ddot{u} \quad (3.17)$$

which is the one-dimensional wave equation, with

$$D_{el} = \frac{k_{nat}}{\rho} \quad (3.18)$$

We can by comparing Equation 3.17 with Equation 3.14 and generalising to 3D, that FEM eigenmodes are precisely the discretely sampled *spatial* solutions of the wave equation.

3.3 Cell growth

We now consider the growth and movement of mesenchymal cells embedded in the ECM. The Oster-Murray mechanism includes a number of mechanochemical factors, but the less well understood ones such as galvanotaxis and haptotaxis are difficult to model without more specific biological knowledge.

In any case the major mode of cell transport is convection by the elastic substrate. An important secondary mode is localised diffusion which equalises cell concentration after mitosis occurs.

3.3.1 Classical diffusion

The random passage of a cell through the ECM can be shown to lead to Fickian diffusion (Murray 1989, Ch. 9.1)(Rubinow 1975, Ch. 5) when there are variations in local cell concentration c

$$\mathbf{J}_{dn} = -D_{dn} \nabla c \quad (3.19)$$

where \mathbf{J} is the cell flux, and the constant of proportionality D_{dn} is known as the diffusion coefficient.

3.3.2 Reaction-diffusion

The general reaction-diffusion expression in Equation 2.1 for one reactant species is

$$\frac{\partial c}{\partial t} = h(c, \mathbf{x}, t) + D_{dn} \nabla^2 c \quad (3.20)$$

In this case the reaction term $h(c, \mathbf{x}, t)$ is simply the cell production rate, since there are no other reactants. The model we use for cell proliferation is the Gompertz function⁶ from Equation 4.1

$$\begin{aligned} h(c, \mathbf{x}, t) &= \frac{dy_{gz}}{dt} \\ &= \frac{d}{dt} \left(a_{gz} e^{-b_{gz} e^{-k_{gz} t}} \right) \end{aligned} \quad (3.21)$$

3.3.3 Conservation of cell mass

We can also arrive at Equation 3.20 by considering the conservation of cell mass. Let the organ volume V be bounded by its surface S . Conservation of cell mass means that the rate of change of cell mass in V is equal to the rate of flow of cell mass across S into V , including cell mass created in V .

This gives

$$\frac{\partial}{\partial t} \int_V c(\mathbf{x}, t) \cdot dV = - \int_S \mathbf{J} \cdot dS + \int_V h_{gz}(t) \cdot dV \quad (3.22)$$

where \mathbf{J}_{dn} is the flux of material, and h is a source of material. Applying the divergence theorem to the surface integral and assuming $c(\mathbf{x}, t)$ is continuous, Equation 3.22 becomes

$$\int_V \left(\frac{\partial c}{\partial t} + \nabla \cdot \mathbf{J} - h_{gz}(t) \right) \cdot dV = 0 \quad (3.23)$$

The integrand must be zero since the organ volume V is arbitrary, giving

$$\frac{\partial c}{\partial t} + \nabla \cdot \mathbf{J} = h_{gz}(t) \quad (3.24)$$

Using classical diffusion as the mechanism of cell redistribution after mitosis

$$\mathbf{J}_{dn} = -D_{dn} \nabla c \quad (3.25)$$

means that Equation 3.24 again becomes (cf. Equation 3.20)

⁶We assume here that for a long time scale and small spatial scale, diffusive redistribution of cells means that mitotic rate is only a weak function of position \mathbf{x} .

$$\frac{\partial c}{\partial t} = h_{gz}(t) + D_{dn} \nabla^2 c \quad (3.26)$$

3.3.4 Local redistribution of cells after mitosis

Equation 3.20 which governs the mitotic growth and localised diffusive redistribution of cells has the solution

$$c(\mathbf{x}, t) = y_{gz}(t) + f_2(\mathbf{x})g_2(t) \quad (3.27)$$

We can now relate the spatial behaviour of cell redistribution $f_2(\mathbf{x})$ to the spatial pressure distribution of the deforming ECM $f_1(\mathbf{x})$.

Substituting for p from Equation 3.13 to Equation 3.12 gives

$$f_1(\mathbf{x})\ddot{g}_1(t) = D_{el}f_1''(\mathbf{x})g_1(t) \quad (3.28)$$

and separating the spatial and temporal components gives

$$D_{el} \frac{f_1''}{f_1}(\mathbf{x}) = \frac{\ddot{g}_1}{g_1}(t) = k_1 \quad (k_1 \text{ arbitrary constant}) \quad (3.29)$$

Doing the same with cell growth and redistribution in Equation 3.20 gives

$$D_{dn} \frac{f_2''}{f_2}(\mathbf{x}) = \frac{\dot{g}_2}{g_2}(t) = k_2 \quad (k_2 \text{ arbitrary constant}) \quad (3.30)$$

3.3.5 Principal modes of growth

Kreysig (1988, Ch. 11.3) shows how boundary conditions constrain k_1 and k_2 to give the same spatial eigenvectors with different eigenvalues. In our model both ECM and cellular distributions will be constrained by epithelial boundaries, so that f_1 and f_2 lead to the same spatial eigenmodes of pressure and cell-concentration distribution respectively. The eigenvalues determine the temporal scaling of the sinusoidal modulation of the ECM substrate, and the exponentially decaying modulation of cell diffusion.

We have shown in Section 3.2.1 that pressure distribution $f_1(\mathbf{x})$ maps directly from the elastic displacement distribution $\mathbf{f}_1(\mathbf{x})$. Cell-concentration differences map in a similar way from the spatial behaviour of cell flux, which gives an analogous cell displacement distribution. The displacement eigenmodes determined from f_1 and f_2 therefore represent the principal spatial modes of mass flux for both ECM and the cell population.

The secretions of fibroblast cells form the ECM, and in our model we implicitly assume that these secretions relieve the elastic strain energy in the ECM as incremental growth takes place. Over the long period of time it takes to achieve a steady state the non-conservative

diffusion of cells will dissipate energy, as will the viscous damping of ECM deformation. The topic of growth energy is examined in Chapter 4.

3.4 Cell-ECM interaction

The Oster-Murray model considers convection of cells by the deforming matrix to be a major mode of cell transport. This occurs concurrently with the mechanisms described in the previous two Sections 3.2–3.3. We now model explicitly the interaction between the deforming ECM and the passively transported cell population using the mass flux due to convection \mathbf{J}_{cv}

$$\mathbf{J}_{cv} = c \frac{\partial \mathbf{u}}{\partial t} \quad (3.31)$$

If we include this in Equation 3.26 which was derived by considering the conservation of cell mass, we get

$$\frac{\partial c}{\partial t} = -\nabla \cdot \left(c \frac{\partial \mathbf{u}}{\partial t} \right) \quad (3.32)$$

We have already shown in Section 3.2 that ECM behaviour is described by

$$\mathbf{u} = \mathbf{f}_1(\mathbf{x})g_1(t) \quad (3.33)$$

and we again postulate a separation of variables solution for c in the case of convective transport

$$c = f_3(\mathbf{x})g_3(t) \quad (3.34)$$

Substituting this into Equation 3.32 gives

$$f_3(\mathbf{x}) \frac{\partial g_3(t)}{\partial t} = -g_3(t) \frac{\partial g_1(t)}{\partial t} \times \nabla \cdot \left(f_3(\mathbf{x})\mathbf{f}_1(\mathbf{x}) \right) \quad (3.35)$$

and rearranging to put temporal terms on the left and spatial terms on the right

$$\begin{aligned} \frac{1}{g_3(t)} \times \frac{\dot{g}_3(t)}{\dot{g}_1(t)} &= -\frac{1}{f_3(\mathbf{x})} \times \nabla \cdot \left(f_3(\mathbf{x})\mathbf{f}_1(\mathbf{x}) \right) \\ &= k_3 \quad (k_3 \text{ arbitrary constant}) \end{aligned} \quad (3.36)$$

The temporal solution is found by separation of variables

$$\frac{\partial g_3(t)}{\partial t} = k_3 g_3(t) \frac{\partial g_1(t)}{\partial t} \quad (3.37)$$

$$\Rightarrow g_3(t) = a_3 e^{k_3 g_1(t)} \quad (3.38)$$

3.4.1 Principal modes of convection

We can in fact see directly from Equation 3.32 that the principal modes of cell convection will occur along the principal modes of ECM deformation. Mass flux \mathbf{J}_{cv} is directed along the vector $\frac{\partial \mathbf{u}}{\partial t}$, but since

$$\frac{\partial \mathbf{u}}{\partial t} = \mathbf{f}_1(\mathbf{x}) \frac{\partial g_1(t)}{\partial t} \quad (3.39)$$

we can see that convective mass transport \mathbf{J}_{cv} must also be directed along the elastic eigenmodes $\mathbf{f}_1(\mathbf{x})$.

3.5 Discussion

We have established the major modes of mass flux in our cell-ECM model of biological growth. These turn out to be the same for elastic ECM deformation and for cell diffusion, since the spatial behaviour of elastic and diffusive structures are the same given the same boundary conditions. In addition the convective mode of cell transport has also been shown to occur along the same modes.

Using linear eigenmodes to describe incremental organ growth also allows us to compute the mass change for each eigenmode. We derive a metric of growth energy in the next Chapter which is a function of mass change.

The Oster-Murray mechanisms we have examined above are applied to a model of organ growth and hence of incremental shape change. In contrast Murray (1989) examines the initiation of spatial pattern formation within fixed boundary conditions. Our model is stable to incremental growth since the mechanisms involved are dissipative and non-conservative. The Oster-Murray model examines unstable eigenmodes which evolve into inhomogeneous but stable distributions of c and u .

3.5.1 Physical parameters

The elastic, diffusive and convective eigenmodes are only the same under the simplifying assumption of uniformly constant distribution of physical parameters - a flat prior. If we have more specific prior information about the spatial distribution of

- mass density and elasticity of ECM
- mass density of and diffusivity of cells
- cell concentration in ECM

then components of mass flux can be separately computed for each mode of transport. With the flat prior the mass flux associated with each eigenmode is only dependant upon the volume change.

Chapter 4

Growth energy

4.1 The Gompertz growth function

Medawar (1940) measured the growth energy of the embryo chicken heart, which was found to follow the Gompertz growth function.

$$y_{gz} = a_{gz} e^{-b_{gz} e^{-k_{gz} t}} \quad (4.1)$$

where a_{gz} , b_{gz} and k_{gz} are constants (subscripts omitted for clarity from now on) and t is the time variable.

Consider the time derivative of y_{gz}

$$\begin{aligned} \dot{y}_{gz} &= akbe^{-kt} e^{-be^{-kt}} \\ &= y_{gz} kbe^{-kt} \end{aligned} \quad (4.2)$$

This leads to the *specific growth rate* R_{gz} as a function of time

$$\begin{aligned} R_{gz} &= \frac{\dot{y}_{gz}}{y_{gz}} \quad (\text{definition}) \\ &= kbe^{-kt} \end{aligned} \quad (4.3)$$

$$\Rightarrow \ln R_{gz} = \ln kb - kt \quad (4.4)$$

From Equation 4.1 we have

$$be^{-kt} = \ln a - \ln y_{gz} \quad (4.5)$$

and we substitute this into Equation 4.3 to give

$$R_{gz} = k \ln a - k \ln y_{gz} \quad (4.6)$$

4.2 Medawar's growth energy

Medawar (1940) determined *growth energy* E_{gz} for the embryo chicken heart by examining the specific amount of growth inhibitor required to cause tissue growth to cease, at a series of different ages. Then assuming growth energy was directly proportional to the amount of inhibitor required, he found a linear trend with negative gradient when plotting $\ln E_{gz}$ against time t

$$\ln E_{gz} = \ln kb - kt \quad (4.7)$$

Medawar also found a linear relationship between E_{gz} and the logarithm of tissue mass $\ln m$

$$E_{gz} = k \ln a - k \ln m \quad (4.8)$$

If we compare Equation 4.7 with Equation 4.4, and also Equation 4.8 with Equation 4.6, we can see that Medawar's growth energy E_{gz} is a measure of specific growth rate R_{gz} , and that the growth of tissue mass m must conform to the Gompertz function¹.

4.3 Growth energy as a function of mass

Rewrite Equation 4.8 using $m_{max} = a$ to represent the fully grown mass at which growth finally halts.

$$\begin{aligned} E_{gz} &= k \ln m_{max} - k \ln m \\ &= k \ln \frac{m_{max}}{m} \end{aligned} \quad (4.9)$$

Figure 4.1 shows a schematic plot of Equation 4.9.

4.4 Interpretation of growth energy metric

In Medawar's experiments E_{gz} represents the the growth potential the organ has left to resist the applied growth inhibitor, which acts by stopping mesenchymal cells (fibroblasts) from redistributing themselves after mitosis. He suggests that this prevents further cell multiplication and hence tissue differentiation and growth.

¹Medawar collected his growth energy data over the range 6–18 days which is equivalent in "physiological time" to a high proportion of the life cycle. Meaningful physical interpretation of Equations 4.7– 4.9 start to fail near the origin of the time and mass axes.

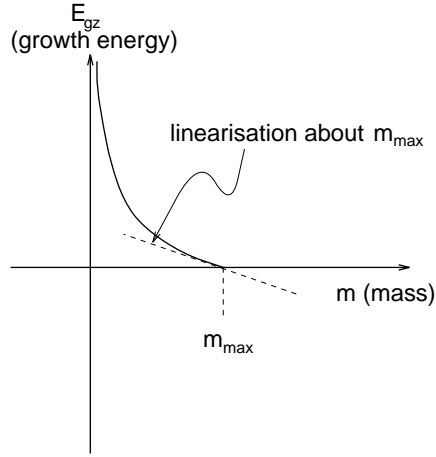


Figure 4.1: Schematic plot of Medawar's growth energy against mass

This is reflected in our use of y_{gz} as the mitotic growth model in Equation 3.21. Growth and shape control mechanisms which act either directly (cf. activator-inhibitor model) or indirectly through the use of mechanical constraints (eg. epithelial boundaries) result in a Gompertzian growth function.

Now consider the change in E_{gz} due to a small change in tissue mass dm

$$\begin{aligned} \frac{dE_{gz}}{dm} &= \frac{-k_{gz}}{m} \\ \Rightarrow \delta E_{gz} &= -k_{gz} \frac{\delta m}{m} \end{aligned} \quad (4.10)$$

This metric describes the change² in internal growth energy which results from incremental growth in tissue mass m .

4.5 Computation of growth energy

We showed in Chapter 3 that mass flux during tissue growth can be described as a linear sum of eigenmodes. This decomposition into principal growth vectors is vital in situations where we have incomplete knowledge of how the organ shape changes in growth, but still need to compute the growth energy of the suggested shape change given by a limited number

²This change is negative since it describes the work done against the inhibitory mechanism.

of homologies between the two shapes. Syn & Prager (1995*a*) describes the use of a locally computed growth energy metric for use in 3D shape registration.

Growth energy can then be optimally approximated by projecting the incomplete shape change vector onto a number of principal growth vectors³, the relative amplitudes of which can be derived using the additional (weighted) global constraint of growth energy minimisation. Syn, Gosling, Berman & Prager (1995) describes the use of this method for the recovery of shape information in 3D ultrasound imaging.

4.6 Eigenmode energy

Consider the tissue growth which results in an incremental shape change, corresponding to a small energetic input which excites all eigenmodes equally.

In general, the ensemble of possible shape changes describes an envelope of variation about the unperturbed shape, the exact distribution of which depends upon the physical characteristics of the cell-ECM model. The principal components transformation of the subspace representing this envelope of variation is therefore represented by the major modes of mass flux in the cell-ECM model. We show this in more detail below, for the ECM model

The principal component modes describe an ordered decomposition of the subspace of variation, into linear eigenvectors which span the spatial variation. The relative proportions of variance represented by each eigenvector are weighted according to the reciprocal of the corresponding eigenvalue.

This is another justification for Section 4.5 in which we describe the use of a small subset of principal growth vectors in growth energy computation: the best choice of n growth vectors is given by the n Principal Component modes which account optimally for spatial variance.

The projection of the incomplete shape change vector onto this set of principal component modes is an under-determined problem which is conditioned by the global constraint which requires the choice which minimises overall growth energy. In the presence of an infinite number of choices, the one which is energetically cheapest is also the most probable.

In fact in (Syn & Prager 1995*a*) we exploit the fact that since our FEM elements are first-order Markov neighbourhoods, a Gibbs-MRF equivalence

$$P(f) \propto e^{-U(f)/T} \quad (T \text{ constant}) \quad (4.11)$$

implies precisely that the least energetic interpolation (minimising U) is also the most probable (maximising P).

³The number of principal growth vectors to be used is determined by computation time, and the Nyquist spatial sampling frequency of the shape model (Syn & Prager 1995*b*)

4.6.1 Statistical modes

Cootes, Taylor, Cooper & Graham (1995) review the use of statistical models of 2D and 3D organ shape variation using principal components analysis of a set of landmark points. Provided enough training information can be obtained - this can be a nontrivial undertaking for 3D landmarks - then this approach offers the advantages of supervised training of the model of linear shape variation.

Martin, Pentland & Kikinis (1994) and Cootes & Taylor (1994) have examined a fusion of the advantages of *a priori* physical models with statistical models. We have shown in an earlier report (Syn & Prager 1994) how the principal components of the statistical model can be initialised from a physical model, and also how the statistical model can be iteratively updated. In this Section we show in more detail the equivalence of the eigenmodes of a physical model, and the principal components of a statistical model of its random perturbation.

The eigenproblem derived from the elastic FEM equilibrium Equation 3.14 is

$$\mathbf{K}\Phi = \mathbf{M}\Omega^2\Phi \quad (4.12)$$

where Φ is the eigenvector matrix and Ω^2 is the diagonal matrix of eigenvalues.

When interpreting Φ as the matrix of principal components this gives the covariance matrix as

$$\Sigma = \Phi\Lambda\Phi^T \quad (4.13)$$

Comparing Equation 4.13 with Equation 4.12, and using $\mathbf{S} = \mathbf{K}^{-1}\mathbf{M}$ from Equation 4.23 gives⁴

$$\Omega^2 = \Lambda^{-1} \quad (4.14)$$

In other words the principal variances in Λ are inversely proportional to the squares of the natural frequencies of the elastic system

$$\lambda_i = \frac{1}{\omega_i^2} \quad (4.15)$$

The matrix pencil (\mathbf{M}, \mathbf{K}) generalises to a system matrix for the cell-ECM model which governs the spatial modes of linearised elastic, diffusive and convective mass flux.

Martin et al. (1994) derive the statistical distribution of elastic eigenmodes for uniform nodal perturbation. We use the alternative assumption mentioned previously of uniform eigenmode excitation.

⁴We assume that the matrix pencil (\mathbf{M}, \mathbf{K}) has been deflated to exclude the rigid-body nullspace, which corresponds to translation- and rotation-normalised principal components analysis. This means that $(\mathbf{M}^{-1}\mathbf{K})$ is full-rank and can be inverted

Uniform eigenmode excitation

Consider a random perturbation \mathbf{r} to an elastic system, which has the steady-state displacement (Syn & Prager 1995*b*)

$$\mathbf{u} = \mathbf{K}^{-1}\mathbf{r} \quad (4.16)$$

Projecting \mathbf{M} and \mathbf{K} onto the \mathbf{M} -orthonormal eigenmodes gives

$$\Phi^T \mathbf{M} \Phi = \mathbf{I} \quad (4.17)$$

$$\Phi^T \mathbf{K} \Phi = \Omega^2 \quad (4.18)$$

Equation 4.18 shows that ω_i^2 is the modal stiffness, so elastic strain energy for an eigenmode of amplitude α_i is proportional to $\omega_i^2 \alpha_i^2$. For each eigenmode to be excited to the same amplitude means that

$$\alpha_i = \frac{\omega_i}{\|\phi_i\|} \quad (4.19)$$

Excitation covariance

The projection of the perturbation vector \mathbf{r} onto the system eigenmodes gives $\mathbf{r}' = \Phi^T \mathbf{r}$, in which the components are the amplitudes of excitation of each eigenmode.

From Equation 4.19 we have the eigenmode variance

$$\sigma_i = \frac{\omega_i^2}{\|\phi_i\|^2} \quad (4.20)$$

The eigenmodes are decoupled, and using the identities established in Equation 4.17–4.18 we have the covariance of \mathbf{r}'

$$\begin{aligned} \Sigma_{\mathbf{r}'} &= (\Phi^T \Phi)^{-1} \Omega^2 \\ &= (\Phi^T \Phi)^{-1} (\Phi^T \mathbf{K} \Phi) \\ &= (\Phi^{-1} \mathbf{K} \Phi) \\ &= (\Phi^T \mathbf{M} \Phi) (\Phi^{-1} \mathbf{K} \Phi) \\ &= \Phi^T \mathbf{M} \mathbf{K} \Phi \end{aligned} \quad (4.21)$$

Since $\mathbf{r}' = \Phi^T \mathbf{r}$ we have

$$\begin{aligned} \Sigma_{\mathbf{r}'} &= \Phi^T \Sigma_{\mathbf{r}} \Phi = \Phi^T \mathbf{M} \mathbf{K} \Phi \\ \Rightarrow \Sigma_{\mathbf{r}} &= \mathbf{M} \mathbf{K} \end{aligned} \quad (4.22)$$

Finally from Equation 4.16 we have the covariance of the system's displacement

$$\begin{aligned}\Sigma_{\mathbf{u}} &= \mathbf{K}^{-1}\Sigma_{\mathbf{r}}\mathbf{K}^{-\mathbf{T}} \\ &= \mathbf{K}^{-1}\mathbf{M}\end{aligned}\tag{4.23}$$

4.7 Biological justification

4.7.1 Tumour growth models

The logistic (cf. Murray et al. 1988), Bertanffy and Gompertz growth functions are generally used in modelling biological growth⁵. All three have been justified on grounds of biological plausibility (Xu 1987, Vaidya & Alexandro 1982) as tumour growth models, and Xu & Ling (1988) have shown using a generalised model which encompasses all three that the Gompertz function is the expectational model given uniform distribution of parameters.

We have bear in mind when citing models of tumour growth that such growths have failed or abnormal growth mechanisms. Xu & Ling include the effects of spatial organisation, surface roughness and competition for nutrition to form a self-limiting growth model which can reasonably be used as a simple approximation to other forms of tissue growth. Such models in the literature are usually of spheroidal growths *in vitro*, which are better suited to organ growth models since there are no additional mechanisms of nutrition or spread as for tumour growth *in vivo*.

4.7.2 Thermodynamic model

Lestienne (1988) reviews the stochastic foundations of the Gompertz function applied to mortality rate distribution⁶. We give here a thermodynamic model of growth control mechanisms, in the context of Medawar's experiment.

If we assume the inhibition energy E_{ib} (cf. Medawar's growth energy E_{gz}) to follow a Boltzmann distribution⁷ then

$$P(E_{ib}) = \frac{1}{T}e^{-(E_{ib}/T)}\tag{4.24}$$

where T is a temperature characteristic which reflects the hostility of the inhibitory control system.

⁵All three can be made to approximate the same sigmoidal plot.

⁶Gompertz originally formulated this function in an actuarial context.

⁷Although Medawar calculated his growth energy E_{gz} by *amount* of chemical inhibitor used - each inhibitory molecule represents a *constant* amount of inhibitory energy - the probability of inhibitory reaction is determined by the kinetic energy of the inhibitory chemical which can be shown to follow a Maxwell-Boltzmann distribution.

Then the cell mitotic rate y_{gz} is directly determined by inhibitory challenges (Shymko & Glass 1976) which meet or exceed the cellular growth energy E_{gz} ,

$$\begin{aligned}
 y_{gz} &= a_{gz} \int_{E_{gz}}^{\infty} P(E_{ib}) . dE_{ib} \\
 &= a_{gz} \frac{1}{T} \int_{E_{gz}}^{\infty} e^{-(E_{ib}/T)} . dE_{ib} \\
 &= a_{gz} e^{-(E_{gz}/T)}
 \end{aligned} \tag{4.25}$$

From Equation 4.7

$$\begin{aligned}
 \ln E_{gz} &= \ln kb - kt \\
 E_{gz} &= k_{gz} b_{gz} e^{-k_{gz} t}
 \end{aligned} \tag{4.26}$$

which we substitute into the Gompertz function in Equation 4.1 to give

$$\begin{aligned}
 y_{gz} &= a_{gz} e^{-b_{gz} e^{-k_{gz} t}} \\
 &= a_{gz} e^{-\frac{b_{gz}}{k_{gz}} E_{gz}}
 \end{aligned} \tag{4.27}$$

We can see by comparing this to Equation 4.25 that the thermodynamic inhibition model leads to the Gompertz growth model.

Chapter 5

Discussion

We have attempted to build a general biological growth model in order to examine and compute the major modes of mass transport and shape change. The mechanisms involved in biological morphogenesis are still poorly understood (Trinkhaus 1984, Ch. 14), and we have limited our model to important and generally accepted mass transport processes. We will continue to update this report as we learn more from experimental investigations and recent literature on theoretical biology.

Anonymous ftp

Technical reports in this series can be obtained via anonymous ftp from our server

`svr-ftp.eng.cam.ac.uk`

World Wide Web

Reports can also be accessed through the Speech, Vision and Robotics Group's web server

`www.eng.cam.ac.uk`

5.1 Acknowledgements

Thanks to Phillip Maini for clarifying aspects of his paper (Murray et al. 1988), to Chris Dance of the SVR Group for help with Chapter 3 and to Stan Sclaroff for Martin et al.'s (1994) report.

Bibliography

- Cootes, T. & Taylor, C. (1994), Combining point distribution models with shape models based on finite-element analysis, in 'Proc. 5th British Machine Vision Conference', BMVA Press, York.
- Cootes, T., Taylor, C., Cooper, D. & Graham, J. (1995), 'Active shape models - their training and application', *Computer Vision and Image Understanding* **61**(1), 38–59.
- Gierer, A. (1974), 'Hydra as a model for the development of biological form', *Scientific American*.
- Goodwin, B., Kauffman, S. & Murray, J. (1993), 'Is morphogenesis an intrinsically robust process?', *Journal of Theoretical Biology* **163**, 135–144.
- Hunding, A. & Engelhardt, R. (1995), 'Early biological morphogenesis and nonlinear dynamics', *Journal of Theoretical Biology* **173**, 401–413.
- Kreysig, E. (1988), *Advanced Engineering Mathematics*, 6th edn, John Wiley and Sons.
- Lestienne, R. (1988), 'On the thermodynamical and biological interpretation of the Gompertzian mortality rate distribution', *Mechanisms of Ageing and Development* **42**, 197–214.
- Levin, S. & Segel, L. (1985), 'Pattern generation in space and aspect', *SIAM Review* **27**(1), 45–67.
- Martin, J., Pentland, A. & Kikinis, R. (1994), Shape analysis of brain structures using physical and experimental modes, Technical Report 276, M.I.T. Media Laboratory, Perceptual Computing.
- Matsushita, M. & Fujikawa, H. (1990), 'Diffusion-limited growth in bacterial colony formation', *Physica A* **168**, 498–508.
- Meakin, P. (1986), 'A new model for biological pattern formation', *Journal of Theoretical Biology* **118**, 101–113.

- Medawar, P. (1940), 'The growth, growth energy, and ageing of the chicken's heart', *Philosophical Transactions of the Royal Society B* **129**, 332–355.
- Meinhardt, H. (1982), *Models of Biological Pattern Formation*, Academic Press, London.
- Meinhardt, H. & Klingler, M. (1987), 'A model for pattern formation on the shells of molluscs', *Journal of Theoretical Biology* **126**, 63–89.
- Moore, K. (1982), *The Developing Human*, 3rd edn, W.B. Saunders.
- Murray, J. (1989), *Mathematical Biology*, Vol. 19 of *Biomathematics Texts*, Springer-Verlag.
- Murray, J., Maini, P. & Tranquillo, R. (1988), 'Mechanochemical models for generating biological pattern and form in development', *Physics Reports* **171**(2), 59–84.
- Rubinow, S. (1975), *Introduction to Mathematical Biology*, John Wiley & Sons.
- Savic, D. (1995), 'Model of pattern formation in animal coatings', *Journal of Theoretical Biology* **172**, 299–303.
- Shymko, R. & Glass, L. (1976), 'Cellular and geometric control of tissue growth and mitotic instability', *Journal of Theoretical Biology* **63**, 355–374.
- Syn, M. & Prager, R. (1994), Mesh models for three-dimensional ultrasound imaging, Technical Report CUED/F-INFENG/TR210, Cambridge University Engineering Department, Trumpington Street, CB2 1PZ.
- Syn, M. & Prager, R. (1995*a*), Bayesian registration of models using FEM eigenmodes, Technical Report CUED/F-INFENG/TR213, Cambridge University Engineering Department, Trumpington Street, CB2 1PZ.
- Syn, M. & Prager, R. (1995*b*), FEM eigenmodes as shape features, Technical Report CUED/F-INFENG/TR211, Cambridge University Engineering Department, Trumpington Street, CB2 1PZ.
- Syn, M., Gosling, J., Berman, L. & Prager, R. (1995), Software for model-based segmentation in three-dimensional freehand ultrasound imaging, Technical Report CUED/F-INFENG/TR214, Cambridge University Engineering Department, Trumpington Street, CB2 1PZ.
- Timoshenko, S. & Goodier, J. (1970), *Theory of Elasticity*, Engineering Societies Monographs, 3rd edn, McGraw-Hill.
- Trinkhaus, J. (1984), *Cells into Organs*, 2nd edn, Prentice-Hall Inc., Englewood Cliffs, N.J.

- Turing, A. (1952), 'The chemical basis of morphogenesis', *Philosophical Transactions of the Royal Society B* **237**, 37–72.
- Vaidya, V. & Alexandro, F. (1982), 'Evaluation of some mathematical models for tumor growth', *International Journal of Biomedical Computing* **13**, 19–36.
- Wolpert, L. (1978), 'Pattern formation in biological development', *Scientific American* **239**(4), 124–138.
- Xu, X.-L. (1987), 'The biological foundation of the Gompertz model', *International Journal of Biomedical Computing* **20**, 35–39.
- Xu, X.-L. & Ling, Y.-B. (1988), 'A study on the expectational model for tumor growth', *International Journal of Biomedical Computing* **22**, 135–141.
- Young, D. (1984), 'A local activator-inhibitor model of vertebrate skin pattenrs', *Mathematical Biosciences* **72**, 51–58.